harmonic confining potential; (2) a position-independent, frequency-dependent drag; and (3) a position-independent, gaussian-distributed, temporally correlated random force. It is not a priori obvious that this decoupling should occur. The fact that it does could be significant for the aerodynamics of nonsteady forces on bluff bodies in turbulent flows—a field of research with many important applications[28].

This work provides an exhaustive demonstration of a steadily driven dissipative system that is perfectly described by near-equilibrium statistical mechanics. Unlike driven systems close to jamming, ours has a single effective temperature that holds at all timescales and that therefore completely describes the fluctuating dynamics. Given this result we can now alter the system, seeking to progressively violate the thermal analogy. Thus, gas-fluidized ping-pong balls could provide an experimental means of addressing the broader challenge of understanding the extent to which near-equilibrium statistical mechanics applies to driven systems. □

Methods

The sphere is a hollow ping-pong ball of mass $m = 2.55$ g, diameter $D = 3.8$ cm, and shell thickness 0.038 cm; including rolling inertial mass, its effective mass is $m_e = m + I/R^2 = 4.22$ g. It rolls without slipping on a flat 12-inch diameter brass sieve, with a wire mesh spacing of 300 μm, and with a 4-inch side wall. Variation of mesh size and height of side wall has little effect. The speed and uniformity of the upflow of air are monitored with a hot-wire anemometer. Here, we work at a flow speed of $U = 280\ \mathrm{cm\ s^{-1}}$; this is below the terminal speed of a falling ping-pong ball ($800\ \mathrm{cm\ s^{-1}}$), and gives a Reynolds number, based on sphere size, of $\mathrm{Re} = 10^4$. Thus, the ball generates turbulence and this kicks it around in the plane. Uniformity of airflow, verified with the anemometer, is achieved by mounting the sieve to a 20 inch × 20 inch × 4 foot tall windbox consisting of two nearly cubical chambers separated by a perforated metal sheet. Air from a blower is introduced through a cloth sleeve connected to an input port on the side of the lower chamber. The windbox is mounted on a motorized tilting platform, which in turn is mounted on a rigid frame with a three-point levelling mechanism. The ball position is measured by a digital camera at a frame rate of 120 Hz. The ball speed and acceleration are found by fitting position versus time to a third-order polynomial, with a fitting window of ±4 points and a gaussian weighting that is nearly zero at the edges. The position resolution is ±0.05 mm. The data in Figs 1–4 are based on 3.9 h of position measurements.

Received 29 May; accepted 16 December 2003; doi:10.1038/nature02294.

1. Hohenberg, P. C. & Shraiman, B. I. Chaotic behavior of an extended system. *Physica D* **37,** 109–115 (1989).
2. Egolf, D. A. Equilibrium regained: From nonequilibrium chaos to statistical mechanics. *Science* **287,** 101–104 (2000).
3. Cugliandolo, L. F. & Kurchan, J. Analytical solution of the off-equilibrium dynamics of a long-range spin-glass model. *Phys. Rev. Lett.* **71,** 173–176 (1993).
4. Herisson, D. & Ocio, M. Fluctuation-dissipation ratio of a spin glass in the aging regime. *Phys. Rev. Lett.* **88,** 257202 (2002).
5. Grigera, T. S. & Israeloff, N. E. Observation of fluctuation-dissipation-theorem violations in a structural glass. *Phys. Rev. Lett.* **83,** 5038–5041 (1999).
6. Berthier, L. & Barrat, J. L. Shearing a glassy material: numerical tests of nonequilibrium mode-coupling approaches and experimental proposals. *Phys. Rev. Lett.* **89,** 095702 (2002).
7. Segre, P. N., Liu, F., Umbanhowar, P. B. & Weitz, D. A. An effective gravitational temperature for sedimentation. *Nature* **409,** 594–597 (2001).
8. Bellon, L., Ciliberto, S. & Laroche, C. Violation of the fluctuation-dissipation relation during the formation of a colloidal glass. *Europhys. Lett.* **53,** 511–517 (2001).
9. Mueth, D. M. *et al.* Signatures of granular microstructure in dense shear flows. *Nature* **406,** 385–389 (2000).
10. Losert, W., Bocquet, L., Lubensky, T. C. & Gollub, J. P. Particle dynamics in sheared granular matter. *Phys. Rev. Lett.* **85,** 1428–1431 (2000).
11. Reydellet, G., Rioual, F. & Clement, E. Granular hydrodynamics and density wave regimes in a vertical chute experiment. *Europhys. Lett.* **51,** 27–33 (2000).
12. Lemieux, P. A. & Durian, D. J. From avalanches to fluid flow: a continuous picture of grain dynamics down a heap. *Phys. Rev. Lett.* **85,** 4273–4276 (2000).
13. Makse, H. A. & Kurchan, J. Testing the thermodynamic approach to granular matter with a numerical model of a decisive experiment. *Nature* **415,** 614–617 (2002).
14. D'Anna, G., Mayor, P., Barrat, A., Loreto, V. & Nori, F. Observing brownian motion in vibration-fluidized granular matter. *Nature* **424,** 909–912 (2003).
15. Ono, I. K. *et al.* Effective temperatures of a driven system near jamming. *Phys. Rev. Lett.* **89,** 095703 (2002).
16. Jaeger, H. M., Nagel, S. R. & Behringer, R. P. Granular solids, liquids, and gases. *Rev. Mod. Phys.* **68,** 1259–1273 (1996).
17. Duran, J. *Sands and Powders, and Grains: An Introduction to the Physics of Granular Materials* (Springer, New York, 2000).
18. Geldart, D. *Gas Fluidization Technology* (Wiley, New York, 1986).
19. Pouligny, B., Malzbender, R., Ryan, P. & Clark, N. A. Analog simulation of melting in two dimensions. *Phys. Rev. B* **42,** 988–991 (1990).
20. Ippolito, I., Annic, C., Lemaitre, J., Oger, L. & Bideau, D. Granular temperature: experimental analysis. *Phys. Rev. E* **52,** 2072–2075 (1995).
21. Olafsen, J. S. & Urbach, J. S. Clustering, order, and collapse in a driven granular monolayer. *Phys. Rev. Lett.* **81,** 4369–4372 (1998).
22. Feitosa, K. & Menon, N. Breakdown of energy equipartition in a 2D binary vibrated granular gas. *Phys. Rev. Lett.* **88,** 198301 (2002).
23. Baxter, G. W. & Olafsen, J. S. Gaussian statistics in granular gases. *Nature* **425,** 680 (2003).
24. Prentis, J. J. Experiments in statistical mechanics. *Am. J. Phys.* **68,** 1073–1083 (2000).
25. Kubo, R., Toda, M. & Hashitsume, N. *Statistical Physics II: Nonequilibrium Statistical Mechanics* (Springer, New York, 1991).
26. Achenbach, E. Vortex shedding from spheres. *J. Fluid Mech.* **62,** 209–221 (1974).
27. Suryanarayana, G. K. & Prabhu, A. Effect of natural ventilation on the boundary layer separation and near-wake vortex shedding characteristics of a sphere. *Exp. Fluids* **29,** 582–591 (2000).
28. Leweke, T., Bearman, P. W. & Williamson, C. H. K. Special issue on bluff body wakes and vortex-induced vibrations—Preface. *J. Fluids Struct.* **15,** 377–378 (2001).

Supplementary Information accompanies the paper on **www.nature.com/nature**.

Acknowledgements We thank L. Bocquet, R.F. Bruinsma, P.G. de Gennes, J. B. Freund, D. Levine, and M. A. Rutgers for suggestions. This work was supported by the NSF through grants to D.J.D. and A.J.L.

Competing interests statement The authors declare that they have no competing financial interests.

Correspondence and requests for materials should be addressed to D.J.D. (durian@physics.ucla.edu).

A route to high surface area, porosity and inclusion of large molecules in crystals

Hee K. Chae[1]*, Diana Y. Siberio-Pérez[1,2], Jaheon Kim[1], YongBok Go[1], Mohamed Eddaoudi[1], Adam J. Matzger[1,2], Michael O'Keeffe[3] & Omar M. Yaghi[1]

Materials Design and Discovery Group
[1]*Department of Chemistry,* [2]*Macromolecular Science and Engineering, University of Michigan, Ann Arbor, Michigan 48109, USA*
[3]*Department of Chemistry, Arizona State University, Tempe, Arizona 85287, USA*

* Permanent address: Department of Chemistry, Hankuk University of Foreign Studies, Korea

One of the outstanding challenges in the field of porous materials is the design and synthesis of chemical structures with exceptionally high surface areas[1]. Such materials are of critical importance to many applications involving catalysis, separation and gas storage. The claim for the highest surface area of a disordered structure is for carbon, at 2,030 $\mathrm{m^2\ g^{-1}}$ (ref. 2). Until recently, the largest surface area of an ordered structure was that of zeolite Y, recorded at 904 $\mathrm{m^2\ g^{-1}}$ (ref. 3). But with the introduction of metal-organic framework materials, this has been exceeded, with values up to 3,000 $\mathrm{m^2\ g^{-1}}$ (refs 4–7). Despite this, no method of determining the upper limit in surface area for a material has yet been found. Here we present a general strategy that has allowed us to realize a structure having by far the highest surface area reported to date. We report the design, synthesis and properties of crystalline Zn_4O(1,3,5-benzenetribenzoate)$_2$, a new metal-organic framework with a surface area estimated at 4,500 $\mathrm{m^2\ g^{-1}}$. This framework, which we name MOF-177, combines this exceptional level of surface area with an ordered structure that has extra-large pores capable of binding polycyclic organic guest molecules—attributes not previously combined in one material.

The conceptual basis of our strategy can be appreciated by considering a graphene sheet (Fig. 1a). Excision of progressively smaller fragments from this sheet and calculation of their Connolly surface areas[8] (see Methods) shows that exposing the latent edges of

the six-membered rings leads to significant enhancement of specific surface area. Thus the surface area of a single infinite sheet is 2,965 $m^2 g^{-1}$ (calculating both sides; see Methods). For units consisting of infinite chains of poly-*p*-linked six-membered rings (Fig. 1b), the surface area is almost doubled (5,683 $m^2 g^{-1}$).

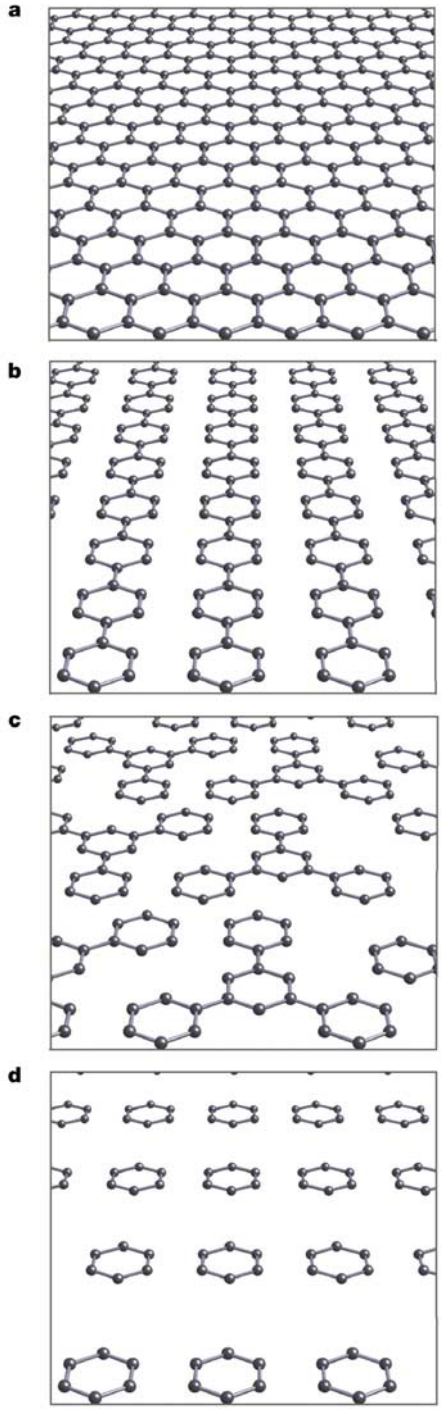

Figure 1 The surface area of graphite fragments. **a**, A graphene sheet extracted from the graphite structure has a Connolly surface area of 2,965 $m^2 g^{-1}$ when calculated in Cerius[2]. **b**, A series of poly-*p*-linked six-membered rings can be extracted from that sheet, thus increasing the surface area to 5,683 $m^2 g^{-1}$. **c**, Excision of six-membered rings 1,3,5-linked to a central ring raises the surface area to 6,200 $m^2 g^{-1}$. **d**, The surface area reaches a maximum of 7,745 $m^2 g^{-1}$ when the graphene sheet is fully decomposed into isolated six-membered rings.

Alternatively, if the graphene sheet is divided into units of three six-membered rings that are 1,3,5-linked to a central ring (Fig. 1c), the surface area is similarly high (6,200 $m^2 g^{-1}$). Finally, exposing all latent edges to give isolated six-membered rings (Fig. 1d) leads to an upper limit value of 7,745 $m^2 g^{-1}$. This analysis does not take into account the hydrogen atoms that would terminate the fragments in metal-organic frameworks (MOFs), although that would result in even higher surface areas for those fragments. Linking these fragments into a real material will not lead to complete realization of these theoretically limiting values. Nevertheless, this analysis suggests that structures with condensed rings should be avoided in order to maximize the number of exposed ring faces and edges.

To put these ideas into practice, we used established reticular chemistry[9] reactions to link the carboxylate derivative (1,3,5-benzenetribenzoate (BTB), a triangular unit of the type shown in Fig. 1c) with basic zinc(II) carboxylate clusters ($Zn_4O(CO_2)_6$, an octahedral unit, see Fig. 2a) into MOF-177. Block-shaped crystals of MOF-177 were produced (see Methods) by heating a mixture of H_3BTB and $Zn(NO_3)_2{\cdot}6H_2O$ in *N*,*N*-diethylformamide (DEF) to 100 °C. The crystals were formulated by elemental analysis as $Zn_4O(BTB)_2{\cdot}(DEF)_{15}(H_2O)_3$ (Calculated: C, 56.96; H, 7.46; N, 7.73. Found: C, 56.90; H, 7.54; N, 7.67). An X-ray diffraction study (see Methods and Supplementary Information) on a crystal isolated from the reaction mixture confirmed this formulation. It also revealed a remarkably open three-dimensional structure of composition $Zn_4O(BTB)_2$, in which each basic zinc acetate cluster is linked to six BTB units (Fig. 2b). In this structure there are 84 exposed edges (60 C–C, 12 C–O, and 12 Zn–O) and only four fused edges (Zn–O) per formula unit (Fig. 2c). The structure of MOF-177 is entirely constructed of six-membered C_6H_4, C_6H_3 and OZn_2CO_2 rings.

There are two places in the structure maximally far from any framework atom. Positions (0,0,0) and (0,0,1/2) have the nearest carbon atom at 7.6 Å and the six positions at (1/2,0,0), etc., have the nearest carbon atom at 7.1 Å. Allowing for a carbon atom van der Waals radius of 1.7 Å, these accommodate spheres of diameter 11.8 and 10.8 Å respectively without touching any framework atoms. The latter pores are connected to produce continuous sinuous channels along (1/2,0,*z*), (0,1/2,*z*), and (1/2,1/2,*z*) (see Fig. 2c). In the as-prepared material, the cavities are occupied by at least 15 DEF and 3 H_2O guests per formula unit. The space occupied by guests alone is 81% of the cell volume. Indeed, gas sorption studies indicate that this space is accessible to incoming guest species and that the framework maintains its integrity in the absence of guests.

Evidence of guest mobility and framework stability initially came from a thermal gravimetric analysis study. A crystalline sample (2.946 mg) was heated at a constant rate of 5 °C min^{-1} in air from 25 to 600 °C. Two weight-loss steps were observed: the first, corresponding to 47.95%, occurred between 50 and 100 °C, which can be attributed to the loss of guest molecules (calculated 48.17%); the second weight loss of 22.01% above 350 °C is due to decomposition of the framework. The lack of any weight loss between 100 and 350 °C indicated that the framework is thermally stable in air at those temperatures (see Supplementary Information). Comparison of the X-ray powder diffraction patterns of the as-synthesized MOF-177 with samples of the material having completely evacuated pores show that the framework periodicity and structure are still preserved, further confirming the architectural stability of the framework in the absence of guests (see Supplementary Information).

To determine the capacity of this material for the uptake of gases, we measured the gaseous N_2 sorption isotherm on samples of MOF-177 in which the pores were fully evacuated. The isotherm revealed a reversible type I behaviour and showed no hysteresis upon desorption of gas from the pores (Fig. 3). The accessible void space is fully saturated with N_2 molecules at relatively low pressures ($P/P_0 \approx 0.2$) with a total weight uptake of 1,288 mg N_2 per gram of

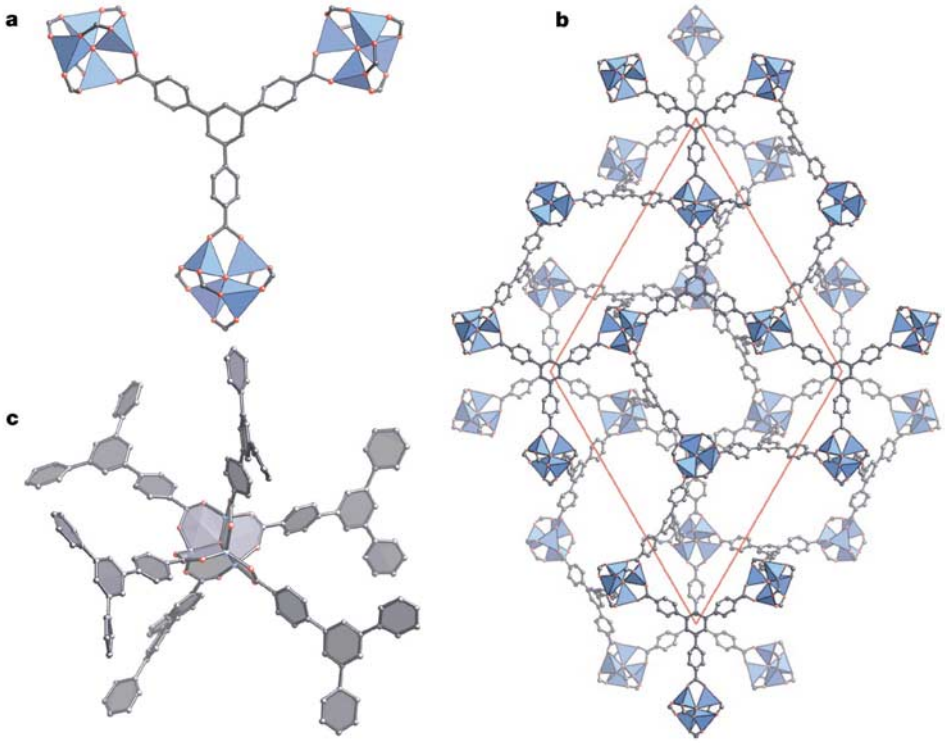

Figure 2 The structure of MOF-177. **a**, A BTB unit linked to three OZn_4 units (H atoms are omitted). ZnO_4 tetrahedra are shown in blue and O and C atoms are shown as red and black spheres, respectively. **b**, The structure projected down [001]. Colours as for **a**. For clarity only about half the *c*-axis repeat unit is shown. **c**, A fragment of the structure radiating from a central OZn_4: six-membered rings are shown as grey hexagons and Zn atoms as blue spheres.

the fully evacuated framework, which correlates to an estimated total number of N_2 molecules of 52.7 per formula unit, and 422 per unit cell.

Using the Dubinin–Raduskhvich equation, we obtained a pore volume of 1.59 $cm^3\,g^{-1}$ (0.69 $cm^3\,cm^{-3}$). By assuming a monolayer coverage of N_2 and applying the Langmuir model, we find the apparent Langmuir surface area to be 4,500 $m^2\,g^{-1}$. The narrowest dimension (10.8 Å) of the pores of MOF-177 is still in the microporous regime (<20 Å diameter pore size). The absolute value of the surface area of all such materials is subject to systematic error arising from standard considerations involving (1) the area assigned to the absorbed molecules and (2) the assumption of monolayer coverage. However, plateaux in isotherms of the type shown in Fig. 3 are invariably interpreted as corresponding to monolayer coverage, so values for different materials, obtained by different groups, are comparable. Nevertheless, the pore volume and surface area of MOF-177 are well beyond those observed for the most porous crystalline zeolites and porous carbon and significantly exceed the previous record[4,9] for a crystalline MOF material (0.59 $cm^3\,cm^{-3}$ and 2,900 $m^2\,g^{-1}$ for MOF-5).

The underlying topology of MOF-177 is a (6,3)-coordinated net with the centre of the octahedral $OZn_4(CO_2)_6$ cluster as the site of six-coordination and the centre of the BTB unit the site of three-coordination. The structure of this net plays an important part in determining pore size by preventing the formation of interpenetrating frameworks. The most regular ('default') (6,3)-coordinated net is 'pyr', named after the pyrite structure[10]. However, two such nets can interpenetrate in such a way that all the rings of one structure are penetrated by the links of the other ('fully catenated') and vice versa, and indeed MOF-150, on the basis of this topology, occurs as an interpenetrating pair of nets (Fig. 4a)[11]. The second net that fully catenates a given net is said to be the dual of that net, and if a net and its dual have the same structure (as in the case of pyr) they are said to be self-dual. Although self-duality is a rare property of nets, it does occur also for default structures of nets with three-, four- and six-coordination, and thus interpenetration of two (or more) copies of identical nets is found to be a common obstacle to synthesis of large-pore materials.

We show here that an effective strategy for avoiding interpenetration is to use nets for which the structure of the dual is very different. The net underlying MOF-177 (Fig. 2b), which we term 'qom', is related to the pyr net. In pyr the six-coordinated sites are arranged as the centres of the spheres in cubic closest packing (that is, on a face-centred cubic lattice); in qom the corresponding

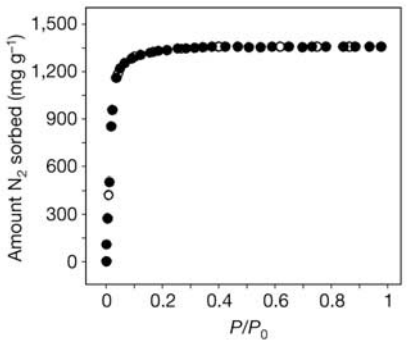

Figure 3 Nitrogen gas sorption isotherm at 78 K for MOF-177 (filled circles, sorption; open circles, desorption). P/P_0 is the ratio of gas pressure (P) to saturation pressure (P_0), with $P_0 = 746$ torr.

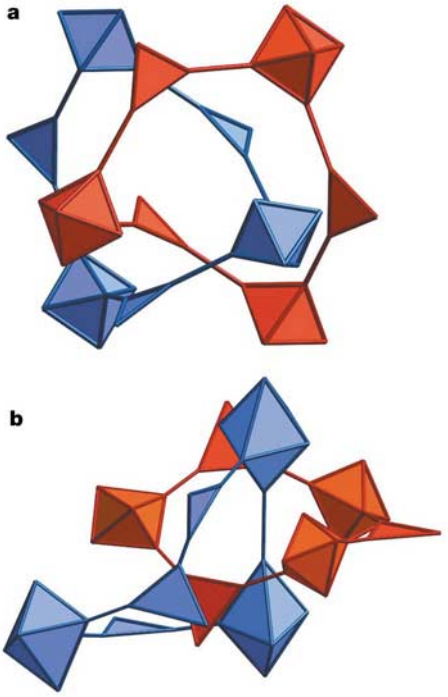

Figure 4 Catenation of rings in nets intergrown with their dual structures. The nets are shown augmented with triangles at the three-coordinated vertices and octahedra at the six-coordinated vertices. **a**, A pair of identical rings in the self-dual pyr net of MOF-150 (ref. 11). **b**, A six-membered ring of the qom net (red) of MOF-177 catenated with a ring of the dual net (blue). A pair of three-coordinated vertices are directly linked, as are pairs of six-coordinated vertices.

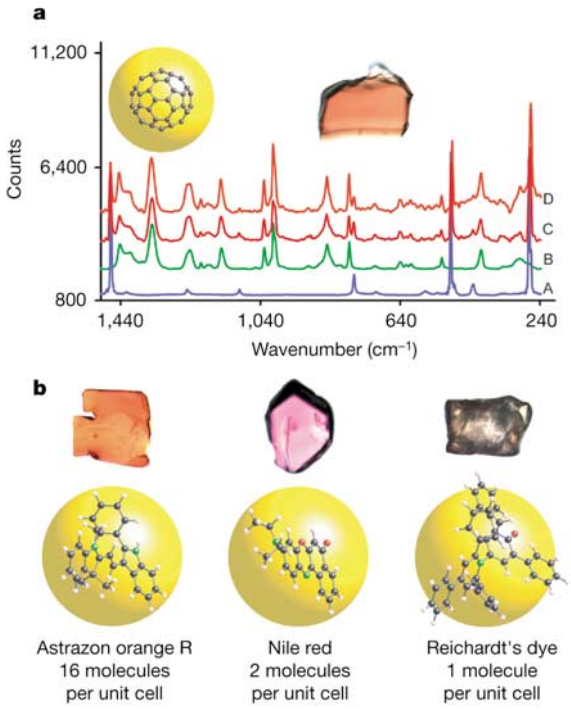

Figure 5 Inclusion of polycyclic organic guests. **a**, Colourless crystals turned deep red, indicating adsorption of C_{60} into MOF-177 single crystals. Analytical evidence was provided by comparison of Raman spectra of a sliced crystal (D) and a whole crystal (C) with bulk C_{60} (A) and an evacuated MOF (B). **b**, The ability of MOF-177 crystals to adsorb large guests was quantified for the dyes Astrazon Orange R, Nile Red and Reichardt's dye. These incorporated 16, 2 and 1 molecules per unit cell, respectively. The ball-and-spoke drawings of the molecules are superimposed on a ball of 11 Å diameter that fits into the pores of MOF-177.

arrangement is that of hexagonal closest packing. However, the dual net, although also (6,3)-coordinated, is very different, and as some of the edges link sites of the same coordination (Fig. 4b) it is not a viable candidate for a MOF. Likewise, as qom is very different from its dual, two such qom nets cannot interpenetrate efficiently. First, we need to identify the strategy for avoiding the pyr net. Simple geometrical arguments show that to prevent formation of the pyr net (as found in MOF-150), when linking octahedral $OZn_4(CO_2)_6$, one should employ aromatic tricarboxylates such as BTB, which is known to have coplanar carboxylates in MOFs[12].

Given the exceptional stability, porosity and large pores of MOF-177, we sought to test its ability to adsorb large organic molecules. Traditionally, inclusion in porous materials has been achieved by either *in situ* synthesis of the guest, synthesis of the framework to entrap the guest or direct incorporation by adsorption[13]. The former two methods are not well suited to making new materials for separations. Furthermore, in all three methods the use of polycrystalline materials raises the concern that inclusion takes place in intercrystalline regions rather than directly in the pores[14]. We have circumvented this concern by using monocrystalline samples of MOF-177 in all studies. Initial studies demonstrated facile uptake of bromobenzene, 1-bromonaphthalane, 2-bromonaphthalene and 9-bromoanthracene from solution (see Methods). However, the uniformity of distribution of these guests in the crystals was difficult to determine directly. Thus we included coloured organic molecules in MOF-177 single crystals so that incorporation of the guest could be directly verified visually[15].

MOF-177 crystals were placed in a C_{60}-toluene solution. After several days the crystals' shape and integrity remained intact and a change in colour to deep red provided optical evidence of C_{60} inclusion in the framework (Fig. 5a). To probe the presence of C_{60}, a MOF-177-C_{60} complex was analysed by Raman spectroscopy. This vibrational spectrum was compared with spectra of bulk C_{60} and with that of evacuated MOF-177. The encapsulated fullerene complex exhibited bands at the same positions as the desolvated MOF-177. However, the fullerene bands were broadened and observed at positions slightly shifted from bulk C_{60}, indicating interaction with the framework (Fig. 5a). Uniformity of inclusion was assessed by slicing a single crystal into three parts, thus exposing the inner core, and verifying that the middle portion was evenly coloured throughout and that the Raman spectrum exhibited bands for both framework and guest (Fig. 5a).

To quantify the ability of MOF-177 to accommodate large polycyclic organic molecules, three dyes, Astrazon Orange R, Nile Red and Reichardt's dye, were selected. We used saturated solutions of these compounds to dye the crystals, and examined a section from the centre of the MOF-177 crystal to gauge the uniformity of dye distribution (Fig. 5b; see Methods). Astrazon Orange R and Nile Red coloured the slices uniformly, indicating free movement of the dye into the crystals. Astrazon Orange R achieved over 40 wt% in the crystals, corresponding to 16 dye molecules in each unit cell. On average, two Nile Red molecules entered each unit cell. The very large molecules of Reichardt's dye, however, penetrated only the outer part of the crystal, with only 1 molecule entering each unit cell on average. Together with the diffusion experiments, these results clearly demonstrate the potential for size selectivity in a regime that is currently inaccessible with conventional porous materials. □

Methods

Surface area calculations

The surface areas for graphite, and fragments of this structure were obtained via the Connolly Surface method[8], as implemented by Cerius[2] 4.2 from Accelrys.

Synthesis of MOF-177

A solution of DEF containing 4,4′,4″-benzene-1,3,5-triyl-tri-benzoic acid (H_3BTB; 5.00×10^{-3} g, 1.14×10^{-5} mol) and $Zn(NO_3)_2\,6H_2O$ (0.020 g, 6.72×10^{-5} mol) was placed in a Pyrex tube of dimensions 10 mm (outer diameter), 8 mm (inner diameter) and 150 mm (length). The sealed tube was heated at a rate of 2.0 °C min^{-1} to 100 °C, held at 100 °C for 23 h, and cooled at a rate of 0.2 °C min^{-1} to room temperature. Block-shaped crystals of MOF-177 were formed and isolated by washing with DEF (4 × 2 ml) and drying briefly in air (~1 min) (0.005 g, 32% based on H_3BTB).

Crystallographic studies on MOF-177

Crystal ($0.30 \times 0.30 \times 0.28$ mm^3) of $Zn_4O(BTB)_2{\cdot}(DEF)_{15}{\cdot}(H_2O)_3$ was sealed in a glass capillary and mounted on a Bruker SMART APEX charge-coupled device diffractometer equipped with a normal focus Mo-target X-ray tube ($\lambda = 0.71073$ Å) operated at 2,000 W power (50 kV, 40 mA). The X-ray intensities were measured at 273(2) K. A total of 1,800 frames were collected with a scan width of 0.3° in ω with an exposure time of 30 s per frame. The frames were integrated with the SAINT software package with a narrow frame algorithm. The integration of the data using a trigonal unit cell yielded a total of 173,392 reflections to a maximum 2θ value of 41.68° of which 12,530 were independent and 5,233 were greater than $2\sigma(I)$. The final cell constants were refined with 5,049 reflections with $4.395 < 2\theta < 41.661$. Analysis of the data showed negligible decay during data collection. Absorption correction was applied by using SADABS. The structure was solved by direct methods and the subsequent difference Fourier syntheses and refined with the SHELXTL (version 6.10) software package, using the trigonal space group $P\bar{3}1c$ (number 163), $a = 37.072(2)$ Å, $c = 30.033(2)$ Å with $Z = 8$ for the formula based on the elemental analysis. There were two independent Zn_4O clusters centred at Wyckoff positions 2*d* and 6*h*: the first of these was disordered over two possible orientations. Final full-matrix least-squares refinement on F^2 converged to $R1 = 0.1538$ ($F > 4\sigma(F)$) and $wR2 = 0.4639$ (all data) with GOF = 1.397. Additional details are presented as Supplementary Information.

Diffusion of bromoarenes

The crystals were transferred from their mother liquor (DMF) to heptane. After 30 min, the heptane was removed and fresh heptane was once again added. This process was repeated three times in order to ensure complete displacement of DMF molecules from the porous framework. The excess heptane was then removed and 1 ml of a heptane solution containing 0.007 M of each of the four bromoarenes was added. The crystals remained immersed in this solution for 90 min. The concentration of each bromoarene in the supernatant liquid was monitored by gas chromatography. The disappearance of material indicates adsorption of bromoarenes by MOF-177 crystals.

Quantification of dye uptake

MOF-177 crystals (3–5 mg) were placed in 0.15 ml of a saturated solution of dye in CH_2Cl_2. During a period of 6 days, the supernatant solution was removed and replaced with fresh dye solution 20 times. After the sixth day of inclusion, the crystals were removed from solution and rinsed three times with CH_2Cl_2. Individual crystals were precisely weighed with a microgram balance and digested in 40 to 60 μl of 0.1 M NaOH in methanol. This solution was quantitatively transferred to a 2 ml volumetric flask and methanol was added to obtain precise dilution. Ultraviolet–visual spectrum absorbance analysis of the resulting solutions allowed for determination of the concentrations of the dyes and thus for the amount of dye included in the MOF-177 framework.

Received 9 September; accepted 16 December 2003; doi:10.1038/nature02311.

1. Davis, M. E. Ordered porous materials for emerging applications. *Nature* **417,** 813–821 (2002).
2. Nijkamp, M. G., Raaymakers, J. E., van Dillen, A. J. & de Jong, K. P. Hydrogen storage using physisorption-materials demands. *Appl. Phys. A* **72,** 619–623 (2001).
3. Chester, A. W., Clement, P. & Han, S. Faujasite zeolitic materials. US patent 6,136,291A (24 October 2000).
4. Li, H., Eddaoudi, M., O'Keeffe, M. & Yaghi, O. M. Design and synthesis of an exceptionally stable and highly porous metal-organic framework. *Nature* **402,** 276–279 (1999).
5. Eddaoudi, M. *et al.* Systematic design of pore size and functionality in isoreticular MOFs and their application in methane storage. *Science* **295,** 469–472 (2002).
6. Noro, S. *et al.* Framework engineering by anions and porous functionalities of Cu(II)/4,4′-bpy coordination polymers. *J. Am. Chem. Soc.* **2002,** 2568–2583 (2002).
7. Seki, K., Takamizawa, S. & Mori, W. Design and gas adsorption property of a three-dimensional coordination polymer with a stable and highly porous framework. *Chem. Lett.* **30,** 332–333 (2001).
8. Connolly, M. L. Solvent accessible surfaces of proteins and nucleic acids. *Science* **221,** 709–713 (1983).
9. Yaghi, O. M. *et al.* Reticular synthesis and the design of new materials. *Nature* **423,** 705–714 (2003).
10. Delgado-Friedrichs, O., O'Keeffe, M. & Yaghi, O. M. Three-periodic nets and tilings: regular and quasiregular nets. *Acta Crystallogr. A* **59,** 22–27 (2003).
11. Chae, H. K., Kim, J., Delgado-Friedrichs, O., O'Keeffe, M. & Yaghi, O. M. Design of frameworks with mixed triangular and octahedral building blocks exemplified by the structure of $Zn_4O(TCA)_2$ having the pyrite topology (TCA = 4,4′,4″ tricarboxytriphenylamine). *Angew. Chem. Int. Edn Engl.* **42,** 3907–3909 (2003).
12. Chen, B., Eddaoudi, M., Hyde, T., O'Keeffe, M & Yaghi, O. Interwoven metal-organic framework on a periodic minimal surface with extra-large pores. *Science* **291,** 1021–1023 (2001).
13. De Vos, D. E. & Jacobs, P. A. Zeolite-based supramolecular assemblies. *Stud. Surf. Sci. Catal.* **137,** 957–985 (2001).
14. Sato, K., Nishimura, Y., Honna, K., Matsubayashi, N. & Shimada, H. Role of HY zeolite mesopores in hydrocracking of heavy oils. *J. Catal.* **200,** 288–297 (2001).
15. Kahr, B. & Gurney, R. W. Dyeing crystals. *Chem. Rev.* **101,** 893–951 (2001).

Supplementary Information accompanies the paper on **www.nature.com/nature**.

Acknowledgements Initial phases of this work were carried out by H. Li and scale-up was performed by A. Benin. We are grateful to the NSF and the DOE for support of various aspects of this programme.

Competing interests statement The authors declare that they have no competing financial interests.

Correspondence and requests for materials should be addressed to A. J. M. (matzger@umich.edu), M.O'K. (mokeeffe@asu.edu) or O.M.Y. (oyaghi@umich.edu).

Hydrogenation and cleavage of dinitrogen to ammonia with a zirconium complex

Jaime A. Pool, Emil Lobkovsky & Paul J. Chirik

Department of Chemistry and Chemical Biology, Baker Laboratory Cornell University, Ithaca, New York 14853, USA

Molecular nitrogen is relatively inert owing to the strength of its triple bond, nonpolarity and high ionization potential. As a result, the fixation of atmospheric nitrogen to ammonia under mild conditions has remained a challenge to chemists for more than a century. Although the Haber–Bosch process produces over 100 million tons of ammonia annually[1] for the chemical industry and agriculture[2], it requires high temperature and pressure, in addition to a catalyst[3], to induce the combination of hydrogen (H_2) and nitrogen (N_2). Coordination of molecular nitrogen to transition metal complexes can activate and even rupture the strong N–N bond[4] under mild conditions, with protonation yielding ammonia in stoichiometric[5] and even catalytic yields[6]. But the assembly of N–H bonds directly from H_2 and N_2 remains challenging: adding H_2 to a metal–N_2 complex results in the formation of N_2 and metal–hydrogen bonds or, in the case of one zirconium complex[7], in formation of one N–H bond and a bridging hydride. Here we extend our work on zirconium complexes containing cyclopentadienyl ligands[8,9] and show that adjustment of the ligands allows direct observation of N–H bond formation from N_2 and H_2. Subsequent warming of the complex cleaves the N–N bond at 45 °C, and continued hydrogenation at 85 °C results in complete fixation to ammonia.

Coordination of N_2 to a homogeneous transition metal complex is often an effective strategy for activation of the N–N bond, although few well-defined metal–N_2 complexes are capable of nitrogen fixation[4]. Molybdenum and tungsten N_2 complexes, for example, can be protonated to yield ammonia[5], and recently this approach has been made catalytic with activities rivalling the nitrogenase family of enzymes[6].

Direct observation of N_2 hydrogenation with a homogeneous transition-metal complex under mild conditions has thus far remained elusive. Typically, addition of H_2 to a metal–N_2 complex results in a metal–hydrogen bond with expulsion of free N_2 (ref. 4). One exception is the dinuclear N_2 complex, $[(P_2N_2)Zr]_2(\mu_2,\eta^2,\eta^2\text{-}N_2)$ (where $P_2N_2 = PhP(CH_2SiMe_2NSiMe_2CH_2)_2PPh$, where Ph = phenyl), which reacts over the course of one week with 1–4 atmospheres of H_2 to form one N–H bond and a bridging